Grid-tied photovoltaic system based on PSO MPPT technique with active power line conditioning

Fernando M. de Oliveira, Sérgio A. Oliveira da Silva ✉*, Fábio R. Durand, Leonardo P. Sampaio, Vinícius D. Bacon, Leonardo B.G. Campanhol*

Department of Electrical Engineering, University of Technology – UTFPR-CP, Av. Alberto Carazzai, 1640. CEP. 86.300-000, Cornélio Procópio – PR, Brazil
✉ *E-mail: augus@utfpr.edu.br*

Abstract: This study presents a single-phase grid-tied photovoltaic (PV) system based on a global maximum power point tracking (MPPT) technique, which is performed by means of the particle swarm optimisation (PSO) method. The PSO-based MPPT technique is employed to solve problems related to mismatching phenomena, such as partial shading, in which the PV arrays are commonly submitted. Considering the search of the global maximum power point under partial shading, the effectiveness of the PSO-based MPPT technique is highlighted when compared with the well-known perturb and observe MPPT technique, since both the mentioned MPPT techniques are used to determine the dc-bus voltage reference to ensure a proper grid-tied inverter operation. A current generator algorithm based on a synchronous reference frame is proposed, which operates in conjunction with a dc-bus controller and MPPT algorithms, computing the reference current of the grid-tied inverter. In addition, the current generator controls the energy processed by the PV system to avoid over power rating of the grid-tied inverter, since the active power injection into the grid, reactive power compensation and harmonic currents suppression are carried out simultaneously. The performance and feasibility of the grid-tied PV system are evaluated by means of simulation and experimental results.

1 Introduction

In recent years, increasing attention has been given to electricity generation from alternative and renewable sources, mainly due to the increased demand in electricity consumption, as well as the eminent worldwide appeal to reduce ecological and economic impacts caused by power generation from non-renewable energy sources, such as fossil fuels. For this reason, electrical energy production from renewable energy sources, such as hydropower, biomass, wind, sea, solar, and others, has increased considerably.

Among the many existing renewable energy sources, solar energy has been highlighted, primarily due to its abundance on the Earth's surface. Thus, taking into account this scenario, the use of photovoltaic (PV) systems has become indispensable in distributed power generation.

Grid-connected PV systems are usually composed of PV arrays, such that one or two energy conversion stages are used to perform the interface between the PV array and the utility grid [1–13]. Generally, the voltage level available at the terminals of a given PV array is not as high as desired to allow the use of a single DC–AC converter to inject the power produced by the PV array into the grid [5–8]. In this case, the use of a first conversion stage to step-up the PV array voltage by using DC–DC converters is necessary [7–11]. Thus, in order to decrease the boost ratio required to obtain a high voltage at the first DC–DC conversion stage output, series connections can be used. Therefore, each DC–DC converter contributes a part of the total output voltage and, hence, a lower boost ratio is required [10–13].

A single-phase PV system using a single-stage conversion to inject active power into the utility grid has been presented in [5], while in [14] an additional active power-line filtering function was carried out in conjunction with the active power-line injection. In [14], the perturb and observe (P&O) technique was used to obtain the maximum power point tracking (MPPT) considering the PV array surface under uniform solar radiation. In [12], where the PV

system was composed of two stages of conversion, that is, a cascade connection of the boost (step-up) converter and a full-bridge inverter, the PV array surface was submitted to non-uniform solar radiation. Thus, an MPPT technique based on particle swarm optimisation (PSO) is employed to overcome the problems related to partial shading. In this application, although the active energy produced by the PV system is injected into the grid, the active filtering is not taken into account.

In this paper, the implemented PV system is composed of a single conversion stage, in which the PV array is directly connected to the grid-tied inverter. The algorithm used to perform the MPPT is based on the PSO method. In other words, the presented PSO-based MPPT technique is used for tracking the global maximum power point (GMPP) of the PV array. Different from the MPPT techniques based on the local maximum power point (LMPP), such as the P&O technique [14], a reduction in the effects related to the occurrence of the shadowing phenomena is achieved, improving the overall PV system performance. The proposed PV system algorithm also considers the active power filtering, in order to improve power quality indicators, such as the power factor (i.e. line utilisation factor), harmonic pollution factor, and others [14, 15]. In other words, the aforementioned indicators can worsen due to the increased use of non-linear loads connected to the power supply systems.

Besides the suppression of the load harmonic currents, the active power-line compensating carries out the load reactive power compensation [14–23]. Thus, the proposed PV system can operate as a shunt active power filter (APF) at the same time as the energy produced by the PV array is injected into the grid, meaning that the local loads can consume part or all the active energy produced by the PV system. Therefore, the reference current used to control the grid-tied inverter must be composed of active, reactive and harmonic components. In this case, the reactive and harmonic components are extracted from the load current by using a synchronous reference frame (SRF) based algorithm, whereas the

active component is obtained by means of the dc-bus voltage controller. On the other hand, the voltage reference employed in the dc-bus voltage controller is determined by the PSO-based MPPT technique.

This paper is organised as follows: The overall description of the PV system, the adopted PV model, the algorithm used to generate the current reference of the grid-tied inverter, both the AC-current and the DC-bus voltage controllers and the phase-locked loop (PLL) system are discussed in Section 2. Section 3 describes the MPPT algorithms based on the P&O and PSO methods, and the criteria used to determine the DC-bus voltage reference. In Section 4, the performance and feasibility of the grid-tied PV system are evaluated by means of simulations, as well as by using a laboratory prototype for experimental validation. Finally, the conclusions are presented in Section 5.

2 Description of the PV system

The complete scheme of the single-phase grid-tied PV system is shown in Fig. 1, which includes the PV array, the single-phase full-bridge (1F-B) inverter, the analog-to-digital (A/D) converters, the PLL system, the SRF-based and PSO-based MPPT algorithms, and the DC-bus voltage and AC-current controllers.

In this section, the PV model description and the PLL and SRF-based algorithms are presented, as well as the controllers, whereas the MPPT algorithms are described in the next section.

2.1 PV model description

The solar cell equivalent electrical circuit presented in [24] was adopted in this paper, which is represented by a current source shown in Fig. 2a, where the PV cell output current i_{pv}, the photocurrent I_{ph}, the reverse saturation current I_r, the diode reverse

saturation current I_{rr}, the PV array voltage V_{pv}, and the PV array open circuit voltage V_{oc_pv} are given, respectively, by (1)–(6).

$$i_{pv} = I_{ph} - I_r\left[e^{q((V+i_{pv}R_s)/\eta kT)} - 1\right] - \frac{V + i_{pv}R_s}{R_p} \tag{1}$$

$$I_{ph} = \left[I_{SC} + \alpha(T - T_r)\right]\frac{G}{1000} \tag{2}$$

$$I_r = I_{rr}\left(\frac{T}{T_r}\right)^3 e^{[(qE_g/\eta k)((1/T_r)-(1/T))]} \tag{3}$$

$$I_{rr} = \frac{I_{SC} - (V_{oc}/R_p)}{e^{qV_{oc}/\eta kT_r} - 1} \tag{4}$$

$$V_{pv} = VN_sM_s \tag{5}$$

$$V_{oc\_pv} = V_{oc}N_sM_s \tag{6}$$

where V is the output voltage at PV cell terminals; I_{ph} and I_r are the photocurrent and reverse saturation currents, respectively; R_s and R_p are the series and shunt resistances, respectively; q is the electron charge; η is the ideality factor of the junction p-n; k is the Boltzmann constant; T represents the ambient temperature, in Kelvin; G is the power density of the solar radiation; T_r is the nominal temperature, in Kelvin (298 K); I_{SC} is the short circuit current at standard test conditions (STC) ($T_r = 25°C$, and $G = 1000$ W/m²); α is the temperature coefficient; I_{rr} is the reverse saturation current in STC; E_g is the band gap energy (1.1 eV), V_{oc} is the open circuit voltage of the PV cells; N_s is the number of PV cells; and M_s is the number of the PV arrays connected in series.

The Newton–Raphson numeric method [25] is used to calculate the PV cell current (i_{pv}) given by (1), due to the non-linear relationship between i_{pv} and V. Thus, i_{pv} is achieved by using a calculation routine implemented in the PV model shown in
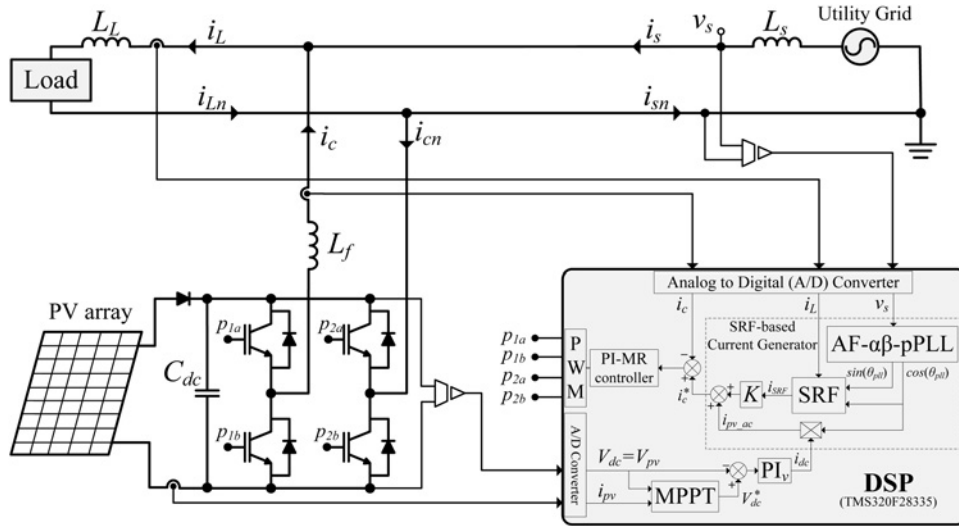

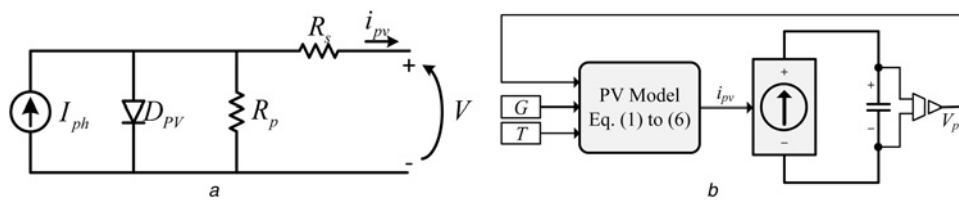**Fig. 1** *Complete scheme of the single-phase grid-tied PV system*

Fig. 2 *PV model*
a Equivalent circuit of the PV cell
b Block diagram of the PV model

Fig. 2b, where the input parameters of the PV model are the output voltage (V_{pv}), power solar radiation (G), and ambient temperature (T), which are obtained in STC [24].

2.2 PV system reference current generation

The PV system reference current must include the active component that represents the energy produced by the PV array, and the reactive and harmonic components of the load. The active component is obtained from the DC-bus voltage controller, whereas the remaining components are obtained using the modified single-phase SRF-based algorithm presented in Fig. 3a, and described in detail in [23]. Based on the fictitious two-phase stationary reference frame, the direct component (d-axis) is given by $id = id_{dc} + id_{h}$, where id_{dc} represents the active fundamental component, and id_{h} is part of the load current harmonic components. On the other hand, the synchronous rotating quadrature current component (q-axis) is given by $iq = iq_{dc} + iq_{h}$, where iq_{dc} represents the reactive fundamental component, and iq_{h} is the remaining part of the load current harmonic components. As can be noted, the fundamental active component is achieved using a 2nd order Butterworth low-pass filter (LPF). In addition, a PLL system estimates the utility grid phase-angle, allowing the generation of the coordinates $\sin(\theta)$ and $\cos(\theta)$, which define the synchronous unit vector used in the SRF-based algorithm, where θ is the estimated phase-angle of the utility voltage ($\theta = \theta_{pll}$). Thus, both the direct and quadrature currents (id, iq) are obtained by (7). As a result, the current i_{SRF} generated by the SRF-based algorithm (Fig. 3a) is given by (8).

$$\begin{bmatrix} i_d \\ i_q \end{bmatrix} = \begin{bmatrix} \cos(\theta_{pll}) & \sin(\theta_{pll}) \\ \sin(\theta_{pll}) & -\cos(\theta_{pll}) \end{bmatrix} \begin{bmatrix} i_\alpha \\ i_\beta \end{bmatrix} \quad (7)$$

$$i_{SRF} = id_{h}\cos(\theta_{pll}) + iq\sin(\theta_{pll}) \quad (8)$$

Finally, the PV system reference current (i_c^*) is given by (9), where $i_{pv\_ac} = i_{dc}\cos(\theta_{pll})$. The output signal obtained from the dc-bus voltage controller (i_{dc}) determines if the PV system will absorb active power from the grid or will furnish active power to the grid. Furthermore, i_{dc} also represents the losses related to both the inductor filter L_f and the switching devices. In other words, i_{dc} controls the total active power demanded by the PV system to regulate the dc-bus voltage.

$$i_c^* = i_{SRF} + i_{pv\_ac} \quad (9)$$

Since the grid-tied inverter is able to handle the active current from the PV system and the reactive and harmonic load currents, simultaneously, the inverter over power rating can occur. In other words, the desired inverter design must guarantee that all active current produced from the PV system is injected into the grid, plus part or all non-active compensation currents generated by the load. Thus, the current i_{SRF} must be limited, such that (10) can replace (9).

$$i_c^* = Ki_{SRF} + i_{pv\_ac} \quad (10)$$

As can be noted, (10) differs from (9) by the insertion of the gain K. This gain, which appears in Fig. 1 and is computed by (11), controls the amplitude of i_{SRF} avoiding an over power rating of the grid-tied inverter.

$$K = \frac{I_{SRFmax}}{I_{SRF}} = \frac{\sqrt{I_{inv}^2 - I_{pv\_ac}^2}}{I_{SRF}} = \frac{\sqrt{I_{inv}^2 - (i_{dc}/\sqrt{2})^2}}{I_{SRF}} \quad (11)$$

where I_{SRFmax} is the maximum allowed rms compensation current and I_{SRF} is the actual rms current obtained from the SRF algorithm shown in Fig. 3a.

On the other hand, the maximum grid-tied inverter rms current (I_{inv}) is given by (12), such that

$$I_{inv} = \sqrt{I_{SRFmax}^2 + I_{pv\_ac}^2} \quad (12)$$

where $I_{pv\_ac} = i_{dc}/\sqrt{2}$ is the PV array rms active current, which is calculated by using the current i_{dc} obtained from the dc-bus voltage controller shown in Fig. 3c.

Thus, from (12) I_{SRFmax} can be calculated as follows

$$I_{SRFmax} = \sqrt{I_{inv}^2 - I_{pv\_ac}^2} \quad (13)$$

Thereby, when $I_{SRF} \leq I_{SRFmax}$ the gain K is set to 1, meaning that the power rate of the grid inverter will not be exceeded. Otherwise, when $I_{SRF} > I_{SRFmax}$, K must be lesser than 1, meaning that the amplitude of the current i_{SRF} must be reduced in order to avoid over power rating of the grid-tied inverter. Fig. 3b presents the gain K against the nominal rms SRF-current (I_{SRF}).

2.3 AC-current and DC-bus control loops

The block diagram of the current controller used to control the 1F-B inverter is shown in Fig. 3c, considering that the current reference i_c^* is achieved from the SRF-current generator presented in Fig. 3a. Based on Fig. 3c, L_f and R_{Lf} are, respectively, the inductance and resistance of the L-filter connected to the grid, and K_{PWM} represents the static gain of the PWM converter, which is calculated considering the peak value of the PWM triangular carrier [26].

Since the compensating reference current i_c^* is not continuous, a proportional-integral multi-resonant (PI-MR) controller [27, 28] is used to control the current synthesised by the 1F-B inverter. Thus, an infinite open loop gain at the resonant frequency (ω_o) is achieved, resulting in null errors in steady state [27].

Thus, the transfer function of the PI-MR controller is given as follows

$$G_{PI-MR}(s) = k_{Pi} + \frac{k_{Ii}}{s} + \sum_{m=1}^{n} \frac{k_{m}s}{(s^2 + (m\omega_1)^2)}$$

$$= G_{PI}(s) + \sum_{m=1}^{n} G_{MR(m)}(s) \quad (14)$$

where k_{Pi} and k_{Ii} represent, respectively, the proportional and integral gains of the current PI controller, k_m represents the resonant gains at a specific resonant frequency, ω_1 is the fundamental frequency, and $m = 1, 3, 5, \ldots, n$.

In this paper $n = 9$, which means that the resonant terms are composed of the 1st, 3rd, 5th, 7th and 9th components. To compensate the load reactive component, as well as the active component injected into the grid, both at fundamental frequency, in (14) the fundamental component ($m = 1$) is considered.

The DC-bus voltage controller is also presented in Fig. 3c. As discussed in Section 2.2, this controller provides the signal i_{dc}, which is used to determine the amplitude of the active current injected into the grid. Thereby, the DC-bus control loop must present reduced bandwidth in order to avoid distortions in reference current (i_c^*).

The PI DC-bus controller gains, k_{Pv} and k_{Iv}, and the PI AC-current controller gains (k_{Pi} and k_{Ii}) presented in (14), are determined using the design procedure presented in [23], which is based on the frequency response method via Bode diagram. This method can be used when the phase margin and the 0 dB gain crossover frequency are employed as design specifications. In addition, the multi-resonant controller gains (k_m) are obtained in order to guarantee that each one of the multi-resonant crossover frequencies (ω_{cm}), related to $G_{MR(m)}$, are equal to the adopted crossover frequency (ω_{ci}) used in the PI AC-current controller design specification, such that $\omega_{cm} = \omega_{ci}$.
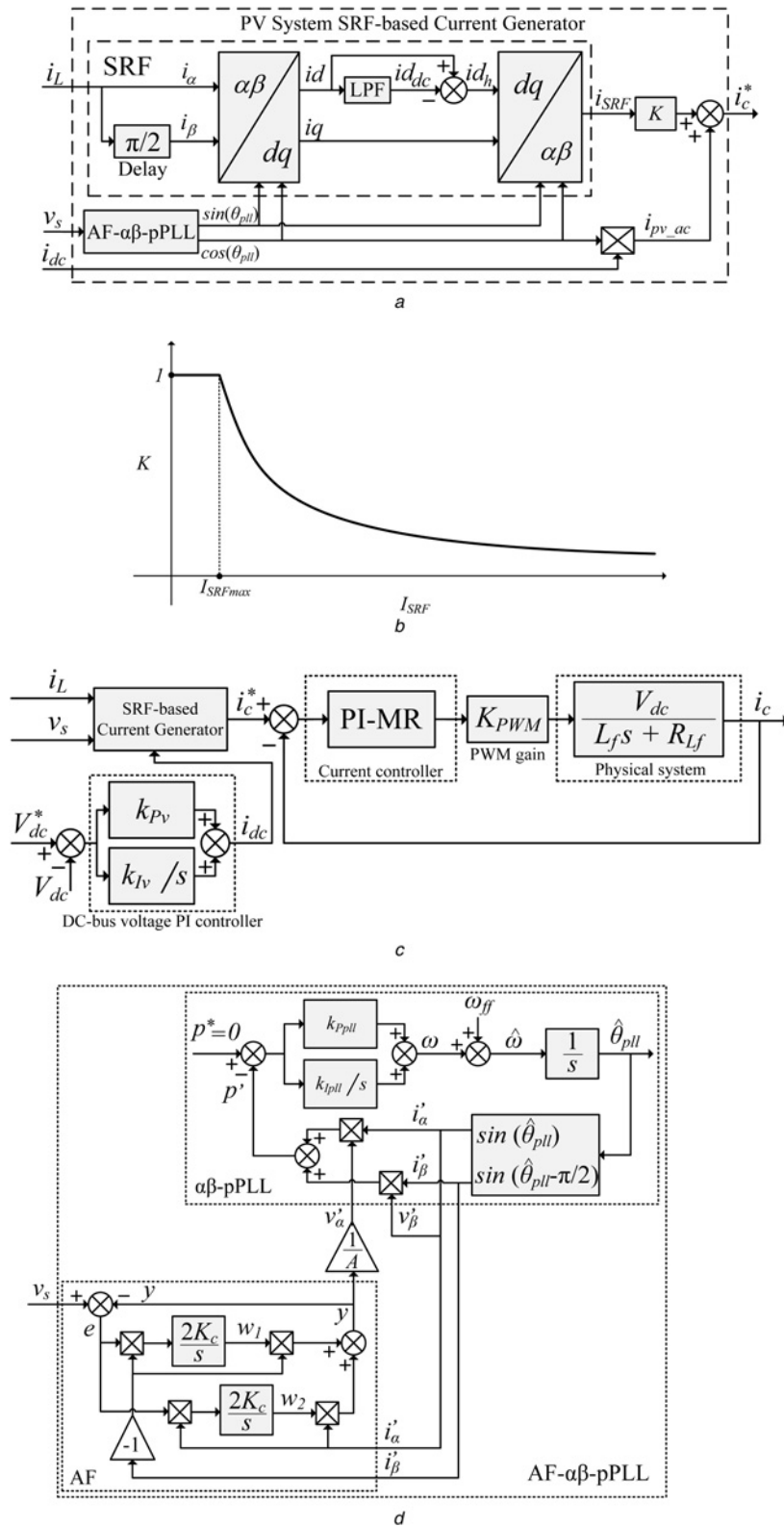
Fig. 3 *PV system*

a Block diagram of the SRF-current generator
b Constant K used to control the power flow through the PV system
c Block diagram of the current control loop and DC-link voltage controller
d Single-phase AF-$\alpha\beta$-pPLL scheme

2.4 Phase-locked loop system

As aforementioned in the previous sections, the PLL system estimates the utility phase-angle that is used to generate the coordinates ($\sin(\theta)$, $\cos(\theta)$) of the unit vector employed in the

SRF-based algorithm, as well as to generate the sinusoidal current (i_{PV}) that composes part of the total PV reference current i_c^*.

Fig. 3d presents the single-phase PLL system implemented in this paper. It uses a non-autonomous adaptive filter (AF) operating together with the $\alpha\beta$-pPLL originating in the AF-$\alpha\beta$-pPLL scheme

presented in detail in [29], where the design requirements and procedures for determining the proportional (k_{Ppll}) and integral (k_{Ipll}) controller gains to guarantee its stability are discussed. This PLL scheme presents good performance when submitted to utility disturbances, such as voltage harmonics, voltage sags/swells, phase-angle jumps and frequency variations. Based on Fig. 3d, AF gain $K_c = \mu/T_s$, where T_s is the DSP sampling time, μ is the adaptation step time, and A is the amplitude of the fundamental utility voltage. The amplitude A is calculated based on the weights w_1 and w_2 of the AF, such that $A = \sqrt{w_1^2 + w_2^2}$ [29].

3 MPPT techniques

In this section the descriptions of MPPT techniques based on PSO and P&O methods are presented. In addition, the criteria used for determining the DC-bus voltage reference are also discussed.

3.1 P&O-based MPPT technique

The implemented P&O MPPT algorithm is presented in Fig. 4a [30], in which a comparison between the current calculated PV power (P_{pv}) and measured PV voltage (V_{pv}) and their previous values is carried out. If both the PV array power and voltage increase, the control increases the voltage reference (V_{dc}^*). On the other hand, if the voltage decreases the voltage reference must also decrease. An inverse logic is adopted when the PV array power decreases. Thus, the MPPT algorithm operates by incrementing or decrementing the voltage reference V_{dc}^* (Fig. 1) to extract the maximum power of the PV array.

An appropriate voltage step size (Δv) must be chosen to assure the good performance of the P&O MPPT technique. Thus, for small Δv,

the state-steady error is reduced. However, when fast changes occur in the environmental conditions, the algorithm can become less efficient. On the other hand, when Δv reaches large values, the losses in steady-state increase due to the oscillations around the MPP [31]. In addition, the P&O MPPT algorithm runs at a constant sampling time ($T_{S_{MPPT}}$) so that small values of $T_{S_{MPPT}}$ imply in fast transients when solar radiation changes occur. On the other hand, large values of $T_{S_{MPPT}}$ make the system slower, causing losses in the power extracted from the PV array [31, 32].

3.2 PSO-based MPPT technique

The PSO method is a population-based stochastic optimisation algorithm for global optimisation [33]. It is based on the behaviour of social groups such as schools of fish or flocks of birds. Due to the fact that it is recursively exploited, an improved performance can be gained by the interactions between individuals, or more specifically by imitation of successful individuals. The movements of the particles are based on (15) and (16) [33, 34].

$$v_i^{k+1} = wv_i^k + \emptyset_1 R_1(Pbest_i - x_i^k) + \emptyset_2 R_2(Gbest - x_i^k) \quad (15)$$

$$x_i^{k+1} = x_i^k + v_i^{k+1} \quad (16)$$

where: v is the adjusted particle speed; w is the inertia weight of the previous velocity in the present speed calculation; $\emptyset_1$ and $\emptyset_2$ are the acceleration coefficients regarding the influences of the best particles and best global positions in the velocity updating, respectively. $Pbest$ and $Gbest$ are the best local and best global position found until the kth iteration by fitness function, respectively; R_1 and R_2 are random variables with uniform distribution; R_1 and $R_2 \in [0, 1]$.
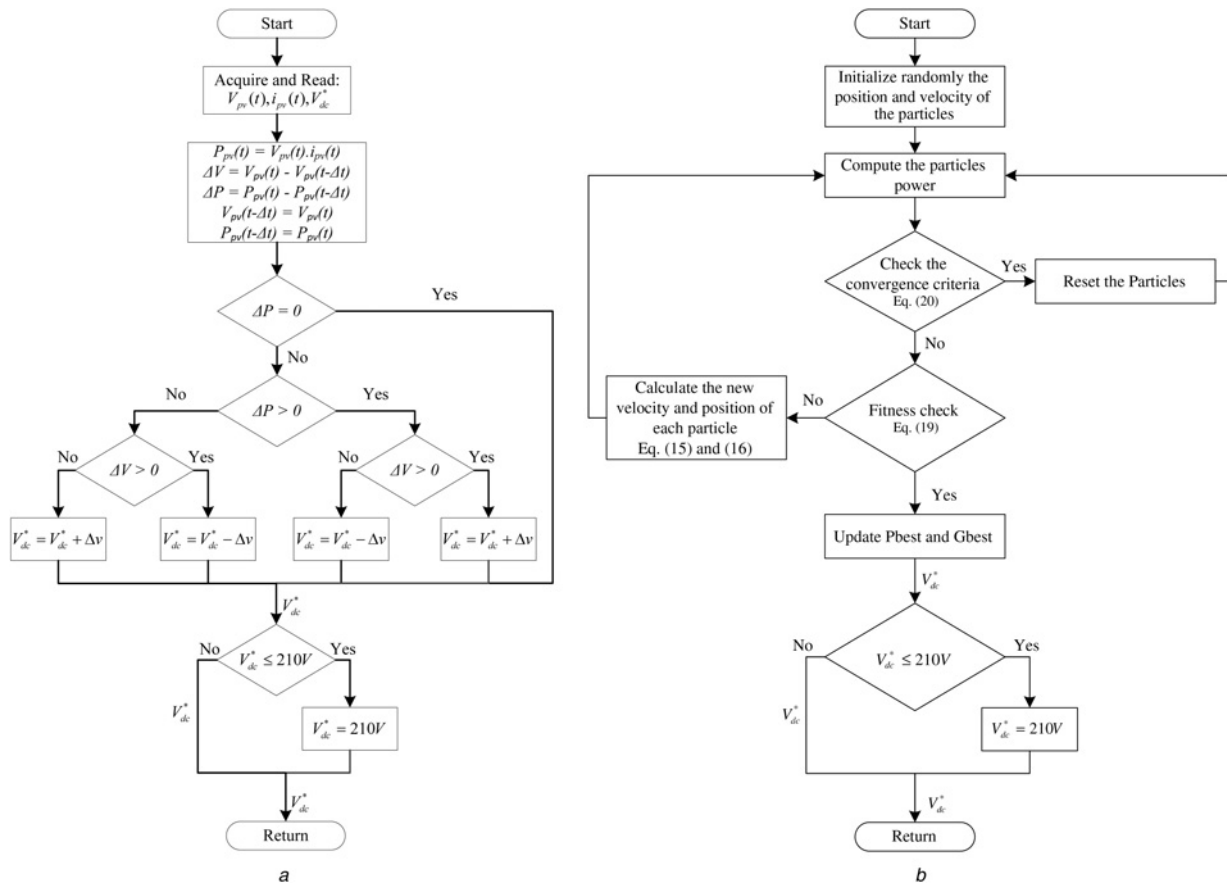

Fig. 4 *MPPT Algorithms*
a Block diagram of P&O MPPT algorithm
b Flowchart of the PSO method applied to the PV system

The algorithm of Fig. 4*b* describes the functioning of the PSO-based MPPT technique applied in this work.

To elaborate further on the inertia weight, it can be observed that a relatively larger value of w is helpful for global optimum, and less influenced by the best global and local positions. On the other hand, a relatively smaller value for w is helpful for convergence, that is, smaller inertial weight encourages the local exploration, such that the particles are more attracted towards Pbest and Gbest. Hence, in order to achieve a balance between the global and local search abilities, a linear inertia weight, which is defined by (17), decreases during the algorithm convergence process, demonstrating good global and local search capabilities in the initial and final iterations, respectively [35].

$$w[k] = \left(w_{\text{initial}} - w_{\text{final}}\right)\left(\frac{\mathcal{G} - k}{\mathcal{G}}\right)^m + w_{\text{final}} \tag{17}$$

where w_{initial} and w_{final} are the initial and final weight inertia, respectively, such that $w_{\text{initial}} > w_{\text{final}}$, $\mathcal{G}$ is the maximum number of iterations, and $m \in [0.6;1.4]$ is the non-linear index [35].

In the PSO-based MPPT, the values of the initial voltage magnitude particles are obtained within the PV system operation range. In addition, the output references (V_{dcn}^*), given by (18), represent the voltages in which the convergence of the method occurs. The PSO convergence is based on the objective function or fitness function. In this work, the objective function compares the current PV power system with the PV power obtained from the previous iteration, as shown by (19). Finally, the restart criterion is defined in (20), and considering $\mathcal{G} \leq 10$, the convergence condition is established.

$$x^k = \begin{bmatrix} V_{\text{dc}1}^{*k} & V_{\text{dc}2}^{*k} & \cdots & V_{\text{dc}n}^{*k} \end{bmatrix} \tag{18}$$

$$P_{pv}^k > P_{pv}^{k-1} \tag{19}$$

$$\frac{P_{\text{pv}}^{k-1} - P_{\text{pv}}^k}{P_{\text{pv}}^k} > \Delta P \tag{20}$$

where n is the number of particles of the PSO method; P_{pv}^{k-1} is the power obtained in the previous iteration; P_{pv}^k is the power obtained in the actual iteration, and ΔP is the minimum relative error. In this work it was considered that $\Delta P = 0.1$, $\emptyset_1 = 1.5$, $\emptyset_2 = 1.2$, $w_{\text{initial}} = 0.9$, and $w_{\text{final}} = 0.4$ according to [35, 36], while the number of particles employed was equal to five. When the PSO method reaches the convergence, the V_{dc}^* chosen is related to the Gbest.

3.3 Criteria for choosing the DC-bus voltage reference

Since the PV system operates by injecting energy into the grid and, simultaneously, acts as APF, the DC-bus voltage must be regulated, such that the minimum DC-link voltage ($V_{\text{dc}_{\min}}$) guarantees a proper operation of the grid-tied inverter. In other words, the dc-bus voltage must be regulated according to the amount of power available in the PV array. Thus, when the power produced by the PV array is enough, considering that the environmental conditions are favourable (solar radiation and temperature), the DC-bus voltage reference V_{dc}^* is always defined by the MPPT algorithm, such that $V_{\text{dc}}^* = V_{\text{MPP}}$ is greater than $V_{\text{dc}_{\min}}$. In this case, the power produced by the PV array is all injected into the grid.

On the other hand, in unfavourable environmental conditions, in which the voltage at the maximum output power conditions (V_{MPP}) is not enough to guarantee the DC-bus voltage, the algorithm defines the DC-bus voltage reference to a constant value ($V_{\text{dc}}^* = V_{\text{MPP}}$), in order to guarantee the system operation.

In this paper, the PV array is comprised of 10 series connected PV modules providing maximum power of around 2.4 kW, where during normal operating conditions, the V_{MPP} is around 308 V ($G = 1000$ W/m^2, $T = 25°$C). On the other hand, taking into account a critical operation condition, such as $G = 100$ W/m^2 and $T = 75°$C, the

Table 1 STC of the solarworld sunmodule plus SW 245 PV array

maximum PV power	$P_{\max} = 245$ W
maximum power point voltage	$V_{\text{mpp}} = 30.8$ V
maximum power point current	$I_{\text{mpp}} = 7.96$ A
open circuit voltage	$V_{\text{oc}} = 37.5$ V
short-circuit current	$I_{\text{sc}} = 8.49$ A

V_{MPP} will be equal to 214 V. Thus, the chosen minimum DC-bus voltage is equal to $V_{\text{dc}_{\min}} = 210$ V to ensure a proper inverter operation, considering the following aspects: (i) peak amplitude of the utility voltage (180 V for nominal utility rms voltage); (ii) losses in both switching devices and passive components (L-filter and DC-bus capacitor); and (iii) DC-bus voltage dynamic when load transients occur. In addition, for partial shading occurrence involving at least three PV modules, the bypass diodes will reduce the operation voltage to around 216 V, such that the choice of $V_{\text{dc}}^* = V_{\text{dc}_{\min}} = 210$ V represents an acceptable voltage level to allow adequate PV system operation.

As can be noted, when the MPPT algorithm operates with constant voltage $V_{\text{dc}}^* = V_{\text{dc}_{\min}}$, the maximum power available in the PV array is not extracted. On the other hand, the PV system continues providing active energy to the grid and performing the active filtering. In cases where the PV array is out, the system remains operating only as a shunt APF, and the DC-bus voltage is controlled using the energy provided from the grid. In this case, the total active energy consumed by the load is drained from the grid.

4 Simulation results

The PV system presented in Fig. 1 is evaluated by means of numerical simulation using a MATLAB/Simulink tool, in which the PV systems inject active energy into the grid and perform

Table 2 Parameters adopted in the simulation and experimental tests

|	
nominal utility rms voltage	$V_s = 127$ V
nominal utility frequency	$f = 60$ Hz
full-bridge converter nominal power	$S_{\text{inv}} = 2540$ VA
nominal rms current of the full-bridge converter	$I_{\text{inv}} = 20$ A
inductive filter	$L_f = 1.5$ mH
inductive filter resistance	$R_{Lf} = 0.48\Omega$
load capacitance	$C = 940$ µF
load resistance	$R = 100\Omega$
nominal load apparent power	$S_L = 380$ VA
load active power	$P_L = 260$ W
fundamental power factor (load)	$PF_1 = 0.99$
power factor (load)	$PF = 0.70$
commutation inductance	$L_L = 1.2$ mH
MPP dc-bus voltage	$V_{\text{dc}} = 308$ V
dc-bus capacitor	$C_{\text{dc}} = 2115$ µF
switching frequency	$f_{\text{sw}} = 20$ kHz
sampling frequency A/D converter	$f_s = 60$ kHz
PWM gain	$K_{\text{PWM}} = 5.33 \times 10^{-4}$
current PI-MR controller gains	$k_{\text{Pi}} = 175.25$; $k_{\text{Ii}} = 29727$; $k_1 = 15700$; $k_3 = 15627$; $k_5 = 15482$; $k_7 = 15265$; $k_9 = 14975$
crossover frequency (current PI controller)	$\omega_{\text{ci}} = 15708$ rad/s
phase-margin (current PI controller)	$PM_i = 89.9°$
dc-bus PI controller gains	$k_{\text{Pv}} = 0.0996$; $k_{\text{Iv}} = 0.0902$
crossover frequency (dc-bus controller)	$\omega_{\text{cv}} = 47.124$ rad/s
phase-margin (dc-bus controller)	$PM_v = 88.9°$
PLL PI controller gains	$k_{\text{Ppll}} = 424.3$; $k_{\text{Ipll}} = 32234$
crossover frequency (PLL PI controller)	$\omega_{\text{c\_pll}} = 430.874$ rad/s
phase-margin (PLL PI controller)	$PM_{\text{pll}} = 80°$
AF gain	$K_c = 420$
cut off frequency (SRF controller) (2nd order LPF Butterworth filter)	$f_c = 30$ Hz
P&O voltage step size	$\Delta v = 1$ V
P&O sampling time	$T_{S_{\text{MPPT}}} = 0.5$ s
PSO minimum error	$\Delta P = 0.1$
PSO acceleration coefficients	$\emptyset_1 = 1.5$; $\emptyset_2 = 1.2$
PSO inertia weights	$w_{\text{initial}} = 0.9$; $w_{\text{final}} = 0.4$
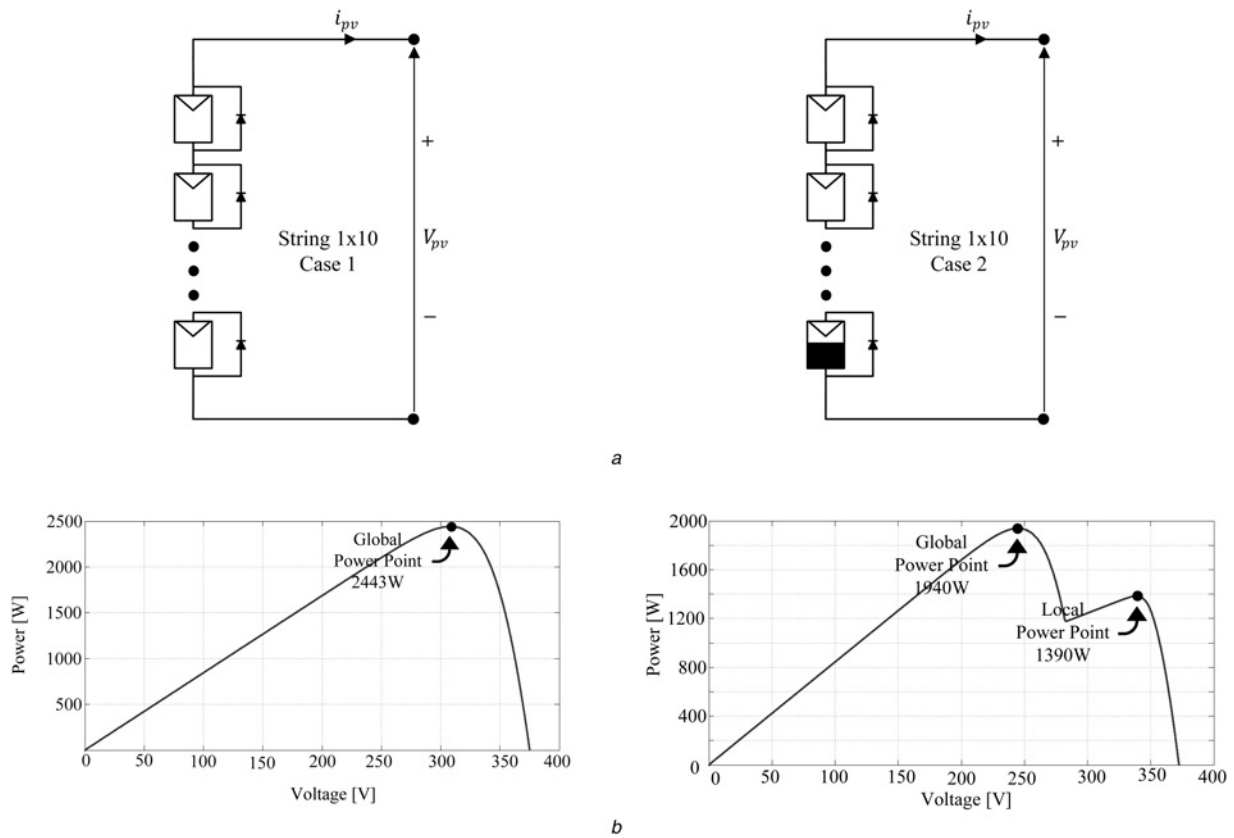
Fig. 5 *PV system*
a PV array considering the Cases 1 and 2
b Characteristic curves for the Cases 1 and 2

active power-line compensation. All parts of the simulated system were discretised, including the SRF and PLL algorithms and controllers. The discretisation is carried out to achieve simulation results as close as possible to the real system. In addition, the delays related to the signal data acquisitions, which are introduced by the anti-aliasing filters and the dead-time of the switching devices were also taken into account in the simulations. The parameters employed in the simulations related to the PV module are presented in Table 1, whereas Table 2 summarises the parameters of the shunt APF and the gains of the PI-MR, PI DC-link, and PI-PLL controllers.

The comparison analysis between the MPPT-based on P&O and PSO are based on the PV array presented in Fig. 5a, whose characteristic curves ($P_{pv} \times V_{pv}$) are shown in Fig. 5b. As can be seen, two solar radiation conditions are considered. In the first, the PV array is submitted to normal atmospheric conditions (Case 1), and in the second, it is submitted to shading conditions (Case 2). As can be noted in Case 1, there is only a GMPP, while in Case 2, apart from the GMPP an LMPP appears.

In Figs. 6a and b, the P&O and PSO MPPT algorithms are evaluated considering Case 1 (uniform solar radiation intensity), where the quantities of voltage and current involved in the PV system operation are shown. As can be observed, both the PSO and P&O MPPT algorithms are able to search the GMPP available in the PV array. Nevertheless, in steady state, the power extracted using the PSO-MPPT algorithm presents reduced oscillations around the maximum point when compared with the P&O-MPPT algorithm. In addition, since the active power-line is performed, even when a non-linear load is connected, the source current (i_s) is almost sinusoidal, as can be seen in Figs. 6a and b, where the source current i_s is shown in the opposite phase with the utility voltage v_s. This means that P_{pv} is higher than the load active power P_L, such that P_{pv} is provided to both utility grid and the load.

Figs. 7a and b present the behaviour of the PV system submitted to the partial shading condition (Case 2). As can be observed, when partial shading occurs, the PSO-based MPPT technique reaches the GMPP, whereas the P&O-based MPPT technique reaches the LMPP. This can occur depending on the operation power point of the PV system. In other words, the P&O-based MPPT technique can track either in the GMPP or in the LMPP, whereas the PSO-based MPPT always reaches the GMPP. As can be seen the source current (i_s) is also almost sinusoidal even when non-linear loads are connected to the grid.

Fig. 7 shows the utility voltage and the active current injected into the grid obtained from the energy extracted from the PV system by using the P&O and PSO MPPT techniques. As can be noted, the amplitude of the injected current (i_c) into the grid is higher, when the PSO-based MPPT technique is used.

By means of the simulation results shown in Fig. 6, it can be observed that both MPPT algorithms reach the GMPP when the PV array is submitted to uniform solar radiation. Although the P&O algorithm reaches the MPP faster than the PSO-based MPPT, it can be observed that higher oscillations appear in steady state. Taking into account the partial shading conditions shown in Fig. 7, despite PSO-based MPPT being slower than the P&O-based MPPT, it can be noted that due to its convergence with the GMPP, the tracking efficiency for extracting the PV power is around 99.95%. On the other hand, since the P&O-based MPPT converges to the LMPP, its tracking efficiency is only 71.93%. The main simulation results used for comparing the performance of the MPPT techniques based on both P&O and PSO are presented in Table 3.

5 Experimental results

This section presents the experimental tests related to the PV system operating with the MPPT technique based on the PSO method, where the digital signal processor (model TMS320F28335, Texas Instruments), shown in Fig. 1, was used to implement the MPPT
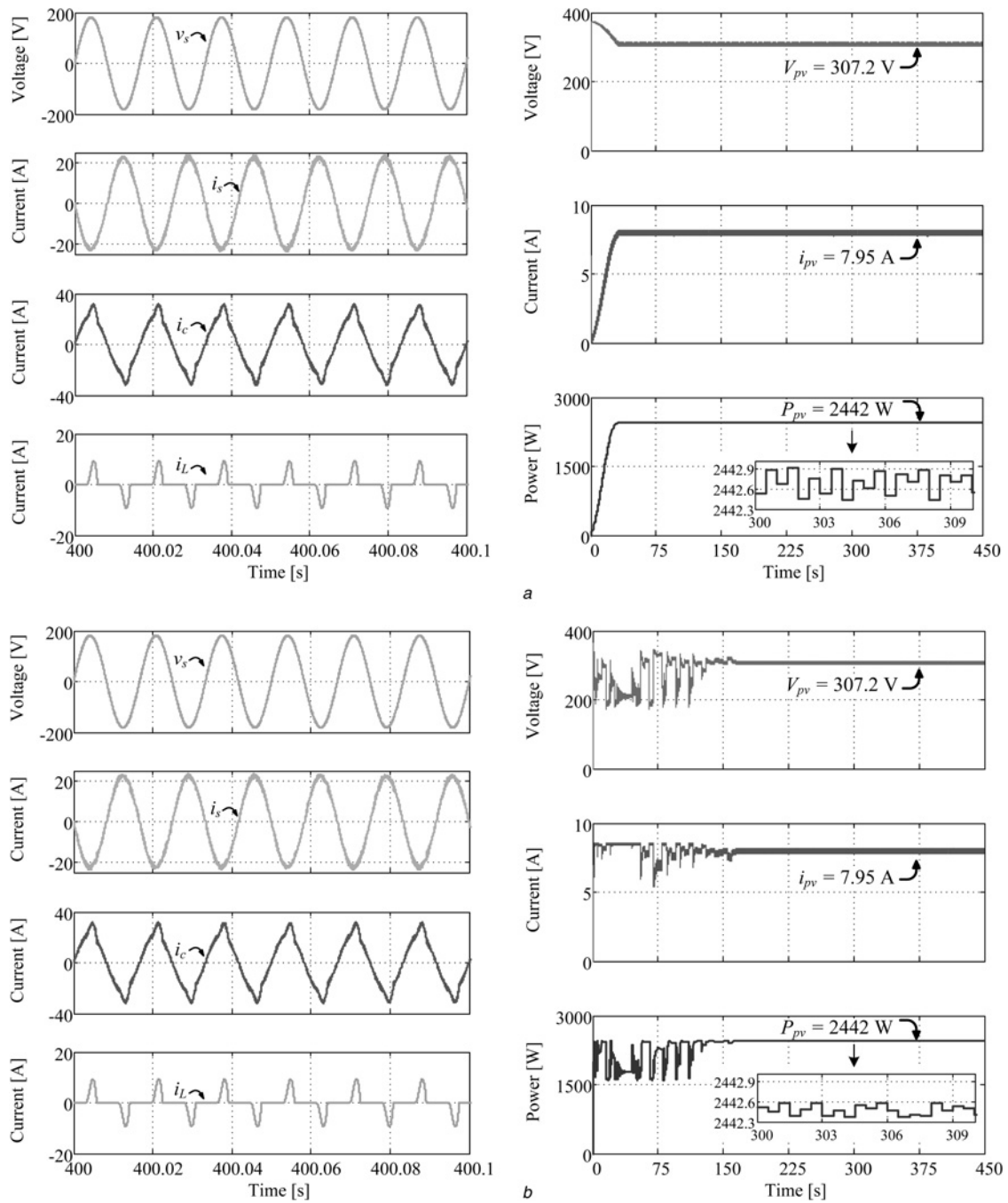
Fig. 6 *PV system*

a Simulation results for the P&O-based MPPT technique (Case 1 – without partial shading condition) – utility voltage v_s, source current i_s, compensating current i_c (inverter current), and load current i_L, PV array voltage V_{pv}, PV array current i_{pv}, and PV array power P_{pv}
b Simulation results for PSO-based MPPT technique (Case 1): Utility voltage v_s, PV system currents (i_s, i_c and i_L), PV array voltage V_{pv}, PV array current i_{pv}, and PV array power P_{pv}

technique, the SRF-current generator, the PLL algorithm and all controllers. A non-linear load composed of a full-bridge diode rectifier followed by RC load was used in the tests, whereas in the full-bridge converter two IGBT modules (SK40GB 123, Semikron) were employed with their proper drivers. The switching frequency of the PWM converter was set at 20 kHz. In addition, three current transducers (model LEM LA 100-P) were used to measure the PV system currents of the PV array, the load and the grid-tied inverter, while the input ac voltage and the dc-link voltage (PV array voltage) were measured using two voltage transducers (model LEM LV 25-P).

Fig. 8a shows the experimental characteristic curve related to the PV array power (P_{pv}) against the time, the PV array quantities (voltage (V_{pv}), current (i_{pv}) and power (P_{pv})), without partial

shading (Case 1). In this condition, the maximum power available in the PV array is around 1770 W. As can be noted, both the MPPT techniques tracked at the MPP (GMPP). In Fig. 8b the same quantities are presented considering the PV array under partial shading (Case 2). As can be observed, the PSO-based MPPT technique reaches the GMPP, whereas the P&O-based MPPT technique reaches the LMPP. The experimental PV system characteristic curves ($P_{pv} \times t$) were obtained by means of the charging of the dc-bus capacitor.

The performance of the PV system operating as an APF is evaluated by means of the experimental results shown in Fig. 9, where the following quantities are presented: source voltage (v_s), source current (i_s), inverter current (i_c) and load current (i_L). Figs. 9a–c refer to the PV system operating using the P&O-MPPT,
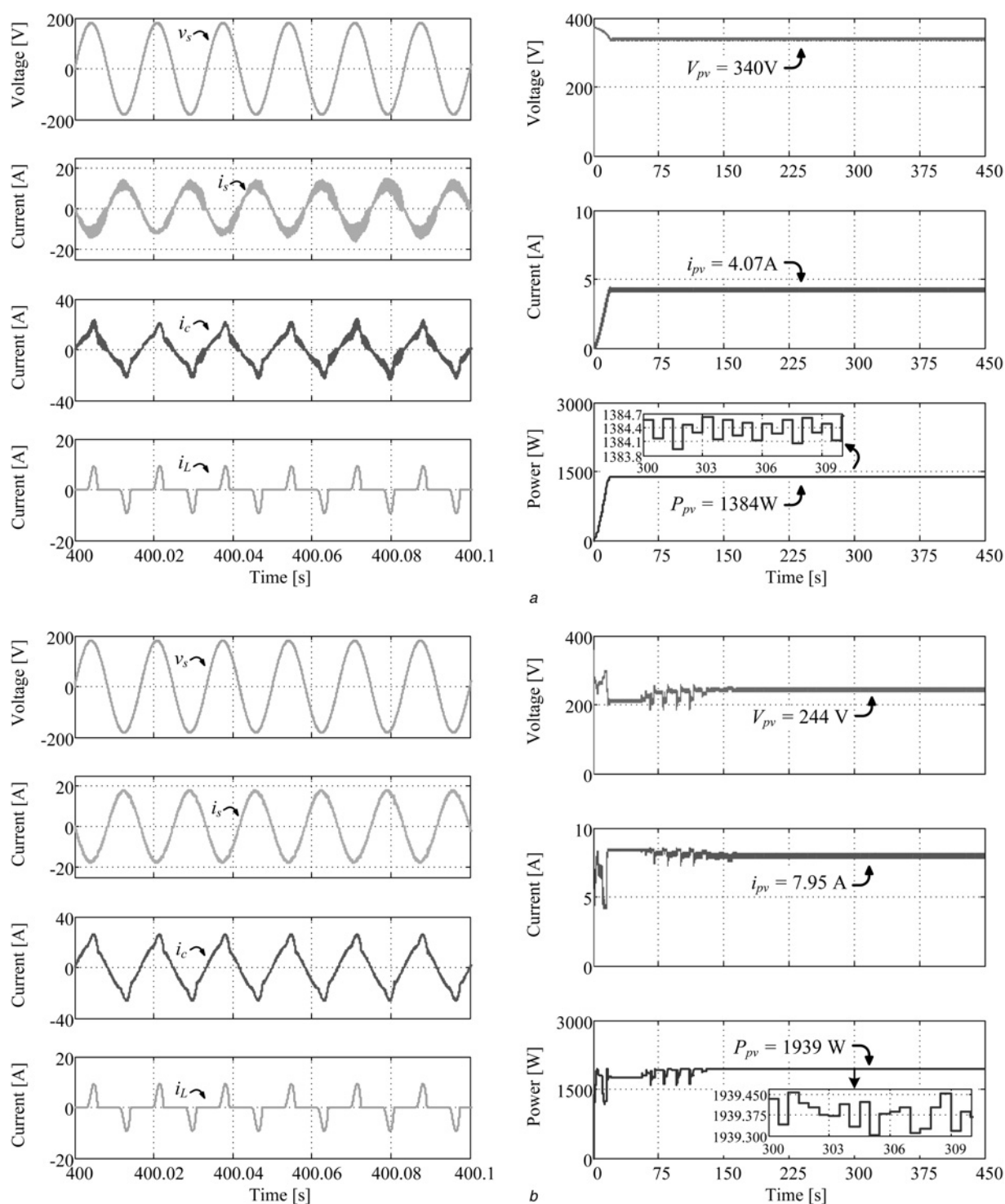
Fig. 7 *Simulation results considering Case 2 (with partial shading condition)*

a P&O-based MPPT technique – Utility voltage v_s, PV system currents i_s, i_c, and i_L, PV array voltage V_{pv}, PV array current i_{pv}, and PV array power P_{pv}
b PSO-based MPPT technique: Utility voltage v_s, PV system currents (i_s, i_c and i_L), PV array voltage V_{pv}, PV array current i_{pv}, and PV array power P_{pv}

Table 3 Main simulation results used to compare the performance of the MPPT techniques based on P&O and PSO

	Without partial shading		With partial shading	
	P&O	PSO	P&O	PSO
time to reach the MPP (s)	15	150	15	150
power oscillation in steady state (%)	0.02	0.009	0.06	0.008
PV power extracted at MPP (W)	2442	2442	1384	1939
tracking efficiency (%)	99.96	99.96	71.93	99.95

while Figs. 9*d–f* refer to the PV system operating using the PSO-MPPT.

Three different tests related to the PV system operation were taken into account, as follows: (i) only active power injection into the grid, considering the non-linear load disconnected (test 1: $P_{pv} > 0$ and $P_L = 0$); (ii) active power filtering (load reactive power compensation and harmonic current suppression) and active power injection into the grid (test 2: $P_{pv} > P_L$); and (iii) only active power filtering (test 3: $P_{pv} = 0$).

In test 1, all the active power produced by the PV array (P_{pv}) is injected into the grid due to the load being disconnected. As can
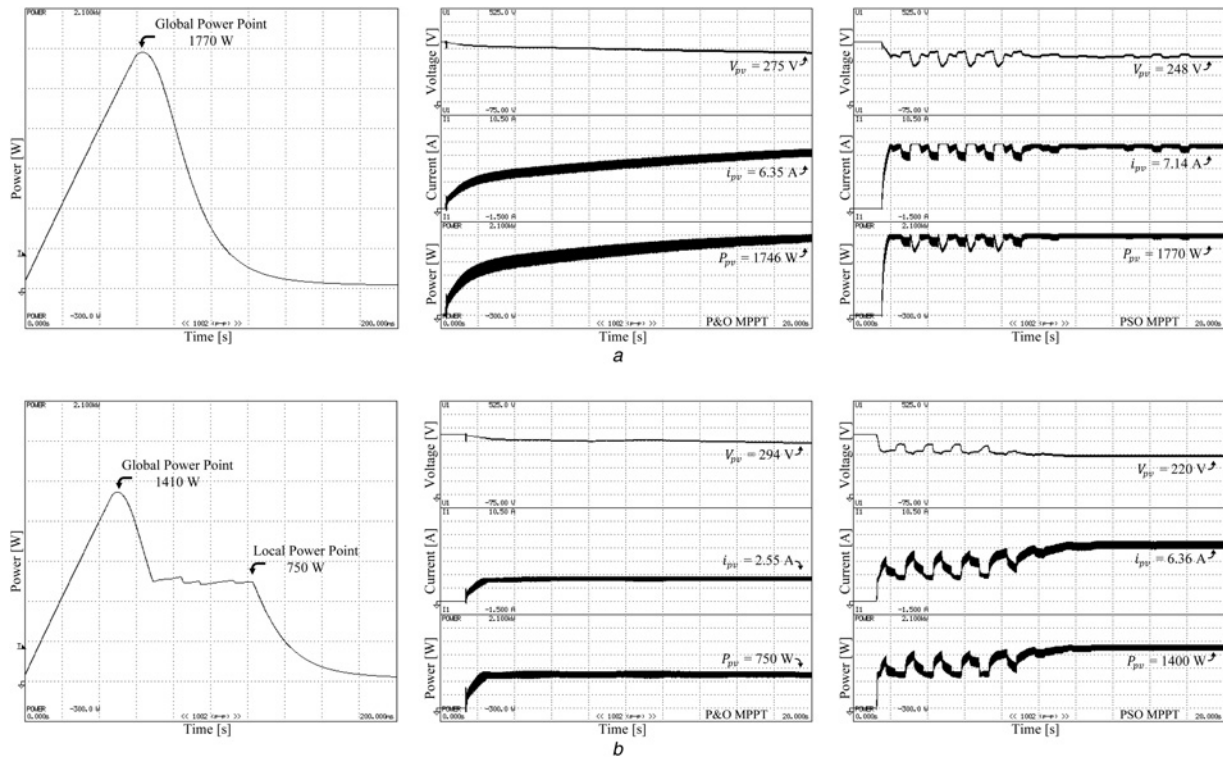
Fig. 8 *Experimental results considering cases 1 and 2*

a Case 1: PV array characteristic curve (300 W/div; 20 ms/div), P&O-based MPPT technique: PV array voltage (V_{pv}), current (i_{pv}), power (P_{pv}) (75 V/div, 1.5A/div, 300 W/div; 2 s/div), and PSO-based MPPT technique: PV array voltage (V_{pv}), current (i_{pv}), power (P_{pv}) (75 V/div, 1.5A/div, 300 W/div; 2 s/div)
b Case 2: PV array characteristic curve (300 W/div; 20 ms/div), P&O-based MPPT technique: PV array voltage (V_{pv}), current (i_{pv}), power (P_{pv}) (75 V/div, 1.5A/div, 300 W/div; 2 s/div), and PSO-based MPPT technique: PV array voltage (V_{pv}), current (i_{pv}), power (P_{pv}) (75 V/div, 1.5A/div, 300 W/div; 2 s/div)

be noted in Figs. 9*a* and *d*, the sinusoidal source current i_s is in opposite phase with the utility voltage v_s; in test 2, the P_{pv} is higher than the load active power P_L. Thus, as can be seen in

Figs. 9*b* and *e*, the PV power (P_{pv}) is provided to the utility grid and load, simultaneously, while the active power filtering is also carried out. Finally, Figs. 9*c* and *f* present the experimental results
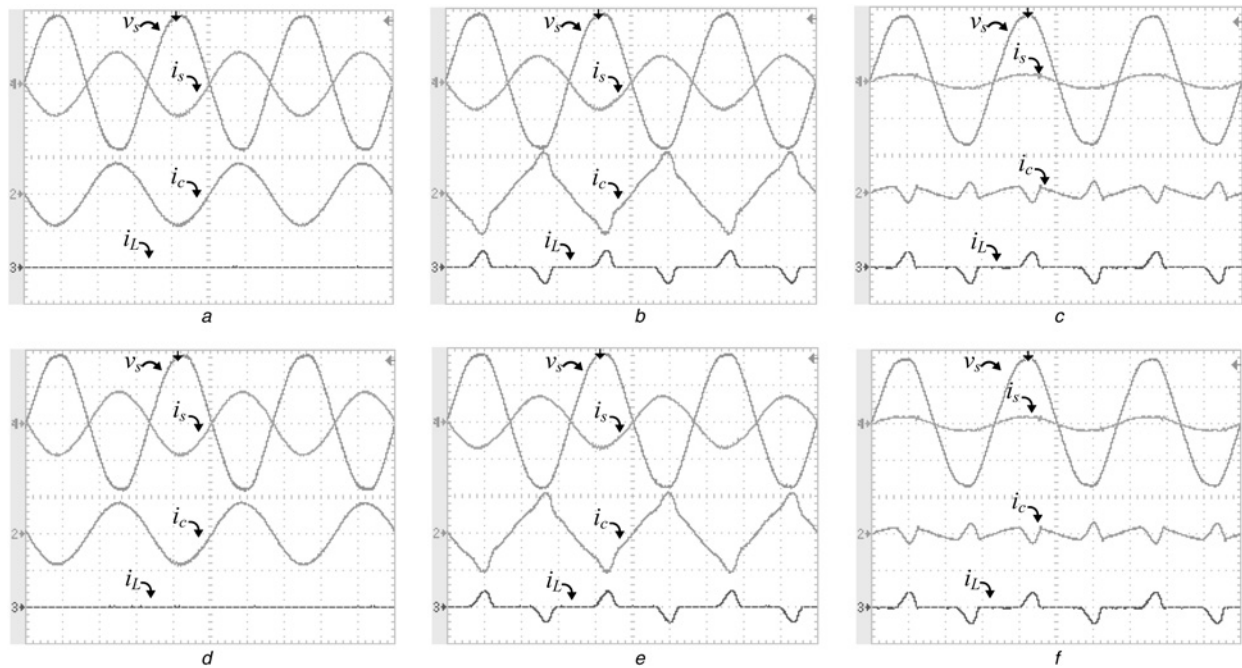

Fig. 9 *PV system performance using P&O MPPT technique (100 V/div, 20A/div, 5 ms/div)*

a Utility voltage v_s and currents i_s, i_c and i_L (test 1: P_{pv} = 1670 W and P_L = 0 W)
b Utility voltage v_s and currents i_s, i_c, and i_L (test 2: P_{pv} = 1700 W and P_L = 260 W)
c Utility voltage v_s and currents i_s, i_c and i_L (test 3: P_{pv} = 0 W and P_L = 260 W); PV system performance using PSO-MPPT technique
d Utility voltage v_s and currents i_s, i_c and i_L (test 1: P_{pv} 1650 W and P_L = 0 W)
e Utility voltage v_s and currents i_s, i_c, and i_L (test 2: P_{pv} = 1670 W and P_L = 260 W)
f Utility voltage v_s and currents i_s, i_c and i_L (test 3: P_{pv} = 0 W and P_L = 260 W)

Table 4 THD of the source and load currents for the load composed of a full-bridge diode rectifier followed by RC load (experimental results)

Tests 1, 2 and 3		(THD %)		(THD %)	
		P&O method		PSO method	
		i_L	i_s	i_L	i_s
1. Active power injection considering the non-linear load disconnected: ($P_{pv} > 0$ and $P_L = 0$)		–	2.2	–	2.0
2. Active power injection into the grid with active power-line filtering: ($P_{pv} > P_L$)		70.2	3.6	70.2	3.5
3. Active power-line filtering (reactive and harmonic current compensation): ($P_{pv} = 0$ and $P_L > 0$)		70.2	9.0	70.2	9.0

Table 5 Main experimental results used to compare the performance of the MPPT techniques based on P&O and PSO

	Without partial shading		With partial shading	
	P&O	PSO	P&O	PSO
time to reach the MPP (s)	175	105	14	118
power oscillation in steady state (%)	10.0	5.1	18.7	7.6
PV power extracted at MPP (W)	1746	1770	750	1400
tracking efficiency (%)	98.6	100.0	52.05	99.93

for test 3, where P_{pv} is null. In this condition, the PV system performs only the active power filtering function.

Table 4 presents the total harmonic distortion (THD) related to the compensated source current i_s considering the three tests imposed to the PV system. As can be observed, the THD of the source current was reduced in all tests, mainly in test 1 ($P_{pv} > 0$ and $P_L = 0$), where the PV system is only injecting active power into the grid ($THD_{i_s} < 5\%$) [37]. In tests 1 and 2 it can be also noted that the source current THDs for the PSO-MPPT are lower than for the P&O-MPPT technique.

Table 5 summarises the main results obtained from the experimental tests involving the MPPT techniques based on P&O and PSO. Similar to the simulation results, the experimental tests show that the PSO-based MPPT operating in partial shading conditions demands more time to reach the GMPP, when compared with the P&O-based MPPT. On the other hand, it presents lower oscillations in steady state. In addition, the MPPT based on PSO presents tracking efficiency around 99.93% at the GMPP, while the tracking efficiency found for the P&O-based MPPT at LMPP is around 55.05%. In other words, although the convergence time of the PSO-based MPPT is higher than the P&O-based MPPT, its efficiency is higher because the GMPP is always reached.

6 Conclusions

This paper presents implementation of a single-phase single-stage grid-tied PV system with active power-line filtering capability. The global MPPT technique was carried out by using the PSO method, in order to overcome mismatching phenomena problems related to partial shading. The PSO-based MPPT technique performance was compared with the MPPT technique based on P&O. Compared with the P&O-MPPT method, the PSO-MPPT was always able to reach the GMPP, allowing the increase of the PV system efficiency.

An SRF-current generator algorithm was proposed to perform the active power injection into the grid and the active power-line conditioning, allowing the load harmonic currents suppression, as well as the load reactive power compensation. Therefore, an effective power factor correction was carried out (unity power factor). Since the PV system handles the active energy produced

by the PV array, as well as the energy used for the active conditioning, a calculation algorithm was proposed, which was integrated into the SRF-based current generator in order to limit the amount of the power processed by the grid-tied inverter. Thus, over power rating of the grid-tied inverter was avoided.

Considering the PV system under partial shading and based on the results obtained by means of simulations and experiments, the grid-tied PV system using the PSO-based MPPT technique presented superior performance when compared with the P&O-based MPPT technique.

7 References

1 Kjaer, S.B., Pedersen, J.K., Blaabjerg, F.: 'A review of single-phase grid-connected inverters for photovoltaic modules', *IEEE Trans. Ind.ustry Appl.*, 2005, **41**, (5), pp. 1292–1306

2 Brito, M.A.G., Sampaio, L.P., Melo, G.A., *et al.*: 'Three-phase tri-state buck–boost integrated inverter for solar applications', *IET Renew. Power Gener.*, 2015, **9**, (6), pp. 557–565

3 Zhou, Y., Huang, W., Zhao, P., *et al.*: 'Coupled-inductor single-stage boost inverter for grid-connected photovoltaic system', *IET Power Electron.*, 2014, **7**, (2), pp. 259–270

4 Xiao, H., Liu, X., Lan, K.: 'Optimised full-bridge transformerless photovoltaic grid-connected inverter with low conduction loss and low leakage current', *IET Power Electron.*, 2014, **7**, (4), pp. 1008–1015

5 Yang, Y., Blaabjerg, F.: 'Low-voltage ride-through capability of a single-stage single-phase photovoltaic system connected to the low-voltage grid', *Int. J. Photoenergy*, 2013, **2013**, pp. 1–9

6 Wu, T.-F., Chang, C.-H., Lin, L-C., *et al.*: 'Power loss comparison of single- and two-stage grid-connected photovoltaic systems', *IEEE Trans. Energy Convers.*, 2011, **26**, (2), pp. 707–715

7 Meneses, D., Blaabjerg, F., García, O., *et al.*: 'Review and comparison of step-up transformerless topologies for photovoltaic ac-module application', *IEEE Trans. Power Electron.*, 2013, **28**, (6), pp. 2649–2663

8 Freitas, A.A.A., Tofoli, F.L., Sá Junior, E.M., *et al.*: 'High-voltage gain dc–dc boost converter with coupled inductors for photovoltaic systems', *IET Power Electron.*, 2015, **8**, (10), pp. 1885–1892

9 Ahmed, M.E.-S., Orabi, M., AbdelRahim, O.M.: 'Two-stage micro-grid inverter with high-voltage gain for photovoltaic applications', *IET Power Electron.*, 2013, **6**, (9), pp. 1812–1821

10 Qahouq, J.A.A., Yuncong, J.: 'Distributed photovoltaic solar system architecture with single-power inductor single-power converter and single-sensor single maximum power point tracking controller', *IET Power Electron.*, 2014, **7**, (10), pp. 2600–2609

11 Walker, R.G., Sernia, C.P.: 'Cascaded dc-dc converter connection of photovoltaic modules', *IEEE Trans. Power Electron.*, 2004, **19**, (4), pp. 1130–1139

12 Rodriguez, J.D.B., Franco, E., Petrone, G., *et al.*: 'Maximum power point tracking architectures for photovoltaic systems in mismatching conditions: a review', *IET Power Electron.*, 2014, **7**, (6), pp. 1396–1413

13 Olalla, C., Deline, C., Clement, D., *et al.*: 'Performance of power-limited differential power processing architectures in mismatched PV systems', *IEEE Trans. Power Electron.*, 2015, **30**, (2), pp. 618–631

14 Wu, T.-Fu, Nien, H.-S., Shen, C.-L., *et al.*: 'A single-phase inverter system for PV power injection and active power filtering with nonlinear inductor consideration', *IEEE Trans. Ind.ustry Appl.*, 2005, **41**, (4), pp. 1292–1306

15 Patidar, R.D., Singh, S.P., Khatod, D.K.: 'Single-phase single-stage grid-interactive photovoltaic system with active filter functions'. Proc. IEEE Power and Energy Society General Meeting, Minneapolis, USA, July 2010, pp. 1–7

16 Campanhol, L.B.G., Silva, S.A.O., Goedtel, A.: 'Application of shunt active power filter for harmonic reduction and reactive power compensation in three-phase four-wire systems', *IET Power Electron.*, 2014, **7**, (11), pp. 2825–2836

17 Todeschini, G., Emanuel, A.E.: 'Wind energy conversion systems as active filters: design and comparison of three control methods', *IET Renew. Power Gener.*, 2010, **4**, (4), pp. 341–353

18 Angulo, M., Ruiz-Caballero, D.A., Lago, J., *et al.*: 'Active power filter control strategy with implicit closed-loop current control and resonant controller', *IEEE Trans. Ind. Electron.*, 2013, **60**, (7), pp. 2721–2730

19 Sladić, S., Skok, S., Nedeljković, D.: 'Efficiency considerations and application limits of single-phase active power filter with converters for photoenergy applications', *Int. J. Photoenergy*, 2011, pp. 1–8

20 Chauhan, S.K., Shah, M.C., Tiwari, R.R., *et al.*: 'Analysis, design and digital implementation of a shunt active power filter with different schemes of reference current generation', *IET Power Electron.*, 2014, **7**, (3), pp. 627–639

21 Buticchi, G., Consolini, L., Lorenzani, E.: 'Active filter for the removal of the dc current component for single-phase power lines', *IEEE Trans. Power Electron.*, 2013, **60**, (10), pp. 4403–4414

22 Patel, H., Agarwal, V.: 'Investigations into the performance of photovoltaics-based active filter configurations and their control schemes under uniform and non-uniform radiation conditions', *IET Renew. Power Gener.*, 2010, **4**, (1), pp. 12–22

23 Angélico, B.A., Campanhol, L.B.G., Silva, S.A.O.: 'Proportional–integral/ proportional–integral-derivative tuning procedure of a single-phase shunt active power filter using Bode diagram', *IET Power Electron.*, 2014, **7**, (10), pp. 2647–2659

24 Rahman, S.A., Varma, R.K., Vanderheide, T.: 'Generalised model of a photovoltaic panel', *IET Renew. Power Gener.*, 2014, **8**, (3), pp. 217–229

25 Greenbaum, A., Chartier, T.P.: 'Numerical methods: design, analysis, and computer implementation of algorithms' (Princeton University Press, New Jersey, 2012)

26 Buso, S., Mattavelli, P.: 'Digital control in power electronics' (Morgan & Claypool Publishers, 2015)

27 Fukuda, S., Yoda, T.: 'A novel current-tracking method for active filters based on a sinusoidal internal model', *IEEE Trans. Ind.ustry Appl.*, 2001, **37**, (3), pp. 888–895

28 Phan, V.-T., Lee, H-H.: 'Control strategy for harmonic elimination in stand-alone DFIG applications with nonlinear loads', *IEEE Trans. Power Electron.*, 2011, **26**, (9), pp. 2662–2675

29 Bacon, V.D., Silva, S.A.O., Campanhol, L.B.G., *et al.*: 'Analysis and performance evaluation of a single-phase phase-locked loop algorithm using a non-autonomous adaptive filter', *IET Power Electron.*, 2014, **7**, (8), pp. 2081–2092

30 Brito, M.A.G., Sampaio, L.P., Galotto, L. Jr. *et al.*: 'Evaluation of the main MPPT techniques for photovoltaic applications', *IEEE Trans. Ind. Electron.*, 2013, **60**, (3), pp. 1156–1167

31 Femia, N., Petrone, G., Spagnuolo, G., *et al.*: 'Optimization of perturb and observe maximum power point tracking method', *IEEE Trans. Power Electron.*, 2005, **20**, (4), pp. 963–973

32 Piegari, L., Rizzo, R.: 'Adaptive perturb and observe algorithm for photovoltaic maximum power point tracking', *IET Renew. Power Gener.*, 2010, **4**, (4), pp. 317–328

33 Kennedy, J., Eberhart, R.: 'Particle swarm optimization'. Proc. Int. Conf. Neural Networks, Perth, Western Australia, December 1995, pp. 1942–1948

34 Miyatake, M., Veerachary, M., Toriumi, F., *et al.*: 'Maximum power point tracking of multiple photovoltaic arrays: a PSO approach', *IEEE Trans. Aerosp. Electron. Syst.*, 2011, **47**, (1), pp. 367–380

35 Chatterjee, A., Siarry, P.: 'Nonlinear inertia weight variation for dynamic adaptation in particle swarm optimization', *Comput. Oper. Res.*, 2006, **33**, (3), pp. 859–871

36 Renaudineau, H., Donatantonio, F., Fontchastagner, J., *et al.*: 'A PSO-based global MPPT technique for distributed PV power generation', *IEEE Trans. Ind. Electron.*, 2015, **62**, (2), pp. 1047–1058

37 IEEE Std. 929–2000: 'IEEE recommended practice for utility interface of photovoltaic (PV) systems', 2000